ACS APPLIED MATERIALS & INTERFACES

Research Article

www.acsami.org

Nitrogen-Doped Porous Carbon Derived from Metal–Organic Gel for Electrochemical Analysis of Heavy-Metal Ion

Lin Cui, Jie Wu, and Huangxian Ju*

State Key Laboratory of Analytical Chemistry for Life Science, School of Chemistry and Chemical Engineering, Nanjing University, Nanjing 210093, People's Republic of China

Supporting Information

ABSTRACT: A nitrogen-doped porous carbon material (N@MOG-C) was prepared by simple pyrolysis of polypyrrole-doped Al-based metal–organic gel (PPy@MOG) at 800 °C. The N@MOG-C possessed a uniform three-dimensional (3-D) interconnected mesoporous structure with a high surface area of 1542.6 m^2 g^{-1} and a large pore volume of 0.76 cm^3 g^{-1}. By using an ionic liquid (IL) to immobilize N@MOG-C on electrode surface, the N@MOG-C was further used for sensitive detection of heavy metal ion. The doping of nitrogen-endowed N@MOG-C with faster electron transfer kinetics than other carbon materials such as MOG-C, multiwalled carbon nanotubes, and graphene. The N@MOG-C-modified electrode showed a high effective area, because of the porous structure. Under optimized conditions, the N@MOG-C-based sensor could detect Cd ions present in concentrations of 0.025–5 μM, with a detection limit of 2.2 nM. The mesoporous structure, fast electron transfer ability, and simple and green synthesis of N@MOG-C made it a promising electrode material for practical applications in heavy-metal-ion sensing.

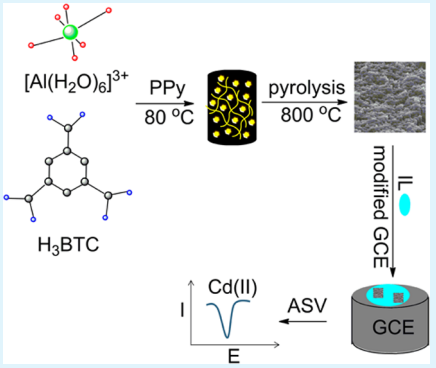

KEYWORDS: *metal–organic frameworks, nitrogen-doped porous carbon material, chemically modified electrode, electrochemical sensor, heavy metal ion, cadmium ion*

INTRODUCTION

Heavy-metal ions are hazardous pollutants to living organisms and can accumulate in the human body through the food chain, leading to adverse effects on the immune, central nervous, and reproductive systems.[1−3] Therefore, the rapid, sensitive, and simple determination of trace heavy metal ions is critical important. Their electrochemical detection has attracted extensive attention, because of their intrinsic advantages of simplicity, good portability, low cost, high sensitivity, and excellent selectivity.[4] Early electroanalytical methods were frequently carried out with hanging mercury drop and mercury-film working electrodes. Considering the toxicity and difficulty involved in the handling of mercury, these electrodes have recently been replaced by mercury-free solid-state electrodes. Nanomaterials, including metal-, carbon-, and silica-based nanomaterials, have been widely used as electrode materials.[5−7] Particularly, the excellent chemical stability, high surface area, versatile structures, high conductivity, and relatively low cost of porous carbon are extremely attractive in electroanalytical application.[7] For this purpose, this work prepared a nitrogen-doped porous carbon material (N@MOG-C) by simple pyrolysis of metal–organic gel (MOG), a new type of extended metal–organic framework (MOF).

MOFs, which consist of metal ions or clusters connected by organic linker groups, are an interesting class of crystalline molecular materials.[8−10] Their structure is versatile and controllable by architecture design and pore functionalization.[11−13] Particularly, their pore size, volume, and functionality are tailorable in a rational manner. Because of the permanent nanoscaled cavities and open channels, MOFs offer congenital conditions for access of small molecules and, therefore, can be an attractive template for the synthesis of porous carbon materials.[14−20] Compared with other porous carbon productions through zeolite or silica templates casting, MOF-based synthesis are less expensive and more environmentally friendly.[21]

Similar to MOFs, MOG possesses desirable characteristics of high surface area, good surface accessibility, and rapid mass transfer or permeability,[22−27] and it has been fabricated by metal–ligand coordination, in conjunction with supramolecular interactions.[28−31] Obviously, MOG can be synthesized under more gentle conditions than MOFs (for example, relatively low reaction temperatures, neutral condition, short reaction time, and routine solvent).[32,33] Thus, it can serve as an attractive template for porous carbon production. For example, a porous carbon material has been synthesized using MOG as a template.[34] This material shows hierarchical porous architecture, ultrahigh surface area, and quite a large pore volume.

Herein, a novel nitrogen-doped porous carbon material was synthesized by using a polypyrrole-doped Al-based MOG

Received: July 4, 2014
Accepted: September 3, 2014
Published: September 4, 2014

   dx.doi.org/10.1021/am504367t | ACS Appl. Mater. Interfaces 2014, 6, 16210–16216

(PPy@MOG) as the template, and that was used as the electrode material for heavy-metal-ion sensing (see Scheme 1).

Scheme 1. Schematic of N@MOG-C and Its Application as Electrode Material for the Sensitive Detection of Cd(II)

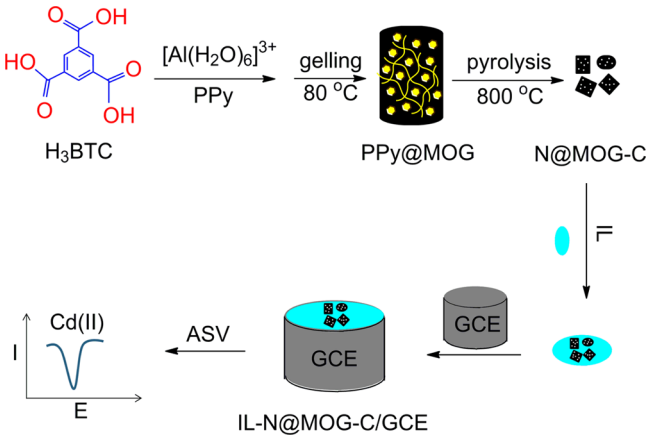

This material, which is defined as N@MOG-C, showed a uniform three-dimensional (3-D) interconnected mesoporous structure with a high surface area and a large pore volume, hence, leading to a high effective area, along with fast electron transfer kinetics of the N@MOG-C-modified electrode, which was favorable to the design of a highly sensitive electrochemical detection method. The excellent performance of the proposed method and the convenient and green preparation of N@MOG-C indicated promising application of the assay in heavy-metal-ion sensing.

EXPERIMENTAL SECTION

Materials and Reagents. Aluminum nitrate nonahydrate ($Al(NO_3)_3{\cdot}9H_2O$) was purchased from Shanghai Sinpeuo Fine Chemical Co., Ltd. (China). 1-Butyl-3-methylimidazolium tetrafluoroborate ionic liquid (IL) (99%), 1,3,5-benzenetricarboxylic acid (H_3BTC), and polypyrrole (PPy) were purchased from Sigma–Aldrich (St. Louis, MO). Cadmium chloride ($CdCl_2{\cdot}2.5H_2O$) was supplied by Alfa Aesar China, Ltd. (China). Acetate buffer solutions (0.1 M) with different pHs were prepared by mixing the stock solutions of 0.1 M sodium acetate (CH_3COONa) and acetic acid (CH_3COOH). Multiwalled carbon nanotubes (MWCNTs, chemical vapor deposition (CVD) method, 98% purity, 40–60 nm in diameter, and 1–2 μm in length) were purchased from Shenzhen Nanotech Port Co., Ltd. (China). Tetraethylene pentamine-functionalized reduced graphene oxide (TEPA@RGO) was purchased from XFNANO Materials Tech Co., Ltd. (Nanjing, China). Other reagents were of analytical grade and used as received. Ultrapure water obtained from a Millipore water purification system (≥18 MΩ, Milli-Q, Millipore) was used in all assays.

Preparation of N@MOG-C. The PPy@MOG was prepared according to the literature, with slight modifications (recall Scheme 1).[33] First, 2.701 g of $Al(NO_3)_3{\cdot}9H_2O$ and 1.512 g of H_3BTC were dissolved in 36 mL of ethanol under vigorous stirring at room temperature. Then, 100 mg PPy was added under ambient conditions. After completely mixing, the resultant homogeneous solution was kept for gelation in an oven at 80 °C for 0.5 h. The resulting gel was allowed to age for 48 h prior to Soxhlet extraction in ethanol to remove the excess unreacted starting materials and subsequently dried overnight at 80 °C to obtain a bulk sample of PPy@MOG. Afterward, PPy@MOG was heated at a rate of 5 °C min^{-1} to 800 °C, followed by pyrolysis at 800 °C for 5 h under N_2. After cooling to room temperature, the resultant black powder was collected and washed with 10 wt % HF aqueous solution. The sample was stirred in HF solution for 24 h and collected by centrifugation. Finally, the product was rinsed with distilled water and dried at 60 °C overnight to obtain N@MOG-C. The MOG and MOG-C were prepared with the similar procedure in the absence of PPy.

Material Characterization Techniques. Transmission electron microscopy (TEM) images were recorded on a Model JEM 2100 high-resolution TEM microscope (JEOL, Japan). Scanning electron microscopy (SEM) images were obtained with a Hitachi Model S-4800 SEM microscope (Japan). X-ray photoelectron spectroscopy (XPS) experiments were conducted using a Model ESCALAB 250 spectrometer (Thermo-VG Scientific Co.; USA) with an ultrahigh vacuum generator. Thermogravimetric analysis (TGA) was performed using a TG-DSC instrument (Netzsch, Model STA 409 PC). Powder X-ray diffraction (XRD) patterns were measured on a Rigaku Model Dmax 2200 X-ray diffractometer with Cu Kα radiation (λ = 1.5416 Å). Nitrogen adsorption–desorption isotherms and pore size distributions were measured at 77 K using a Micromeritics Model ASAP 2020 system.

Electrochemical Characterization. The electrode surface was modified with the following procedure: first, the bare glassy carbon electrode (GCE) was polished with 0.3 and 0.05 μm alumina slurry on microcloth pads, respectively, followed by successive sonication with pure water and ethanol for 3 min, and then drying with nitrogen. Meanwhile, the mixture of 1 mg of N@MOG-C and 50 μL of IL was ground in an agate mortar for ~20 min to obtain IL-N@MOG-C gel. The GCE was coated with IL-N@MOG-C film by rubbing the electrode over the gel. To obtain a homogeneous thin gel film, the coating was further smoothed with a spatula and the modified amount was controlled to 0.5 mg by weighing. Similarly, the IL-MOG-C-, IL-TEPA@RGO-, and IL-MWCNTs-modified GCEs were prepared, respectively.

All of the electrochemical experiments were performed using a Model CHI660D electrochemical workstation (CH Instruments, Inc., USA) with a conventional three-electrode cell, in which the bare or modified GCE (d = 3 mm), the saturated calomel electrode, and platinum wire served as the working electrode, reference electrode, and auxiliary electrode, respectively. Electrochemical impedance spectroscopy (EIS) analysis was performed in 0.1 M KCl containing 5 mM $[Fe(CN)_6]^{3-}/[Fe(CN)_6]^{4-}$.

Square wave anodic stripping voltammetry (SWASV) was used for the detection of Cd(II) with a deposition potential of −1.0 V for 180 s in 0.1 M acetate buffer (pH 5.0). The anodic stripping of electrodeposited metal was performed in the potential range of −1.0 to −0.7 V at the following parameters: frequency, 15 Hz; amplitude, 25 mV; and increment potential, 4 mV.

RESULTS AND DISCUSSION

Characterization of PPy@MOG and N@MOG-C. Both MOG and PPy@MOG showed continuous mass loss from room temperature up to ca. 500 °C (see Figure S1A in the Supporting Information). This could be attributed to the removal of residual ethanol and guest molecule (H_3BTC) entrapped in the porous gel matrix. The weight loss between 425 °C and 525 °C corresponded to the decomposition of the host frameworks. TGA revealed that the pyrolysis of N@MOG could be completed at temperatures higher than 700 °C, which remained 37.79% of the original mass (see Figure S1A, curve b, in the Supporting Information). Compared with the yellow gel matrix of MOG, the PPy@MOG was appeared as a deep black gel matrix (see Figure S1B in the Supporting Information). The doping of PPy did not affect the formation of the gel matrix.

The morphologies of the gel precursors played a critical role in the preparation of carbon products. Although PPy@MOG (Figure 1B) appeared to have larger grains than MOG (Figure 1A), it still exhibited a porous structure, which indicated that the nitrogen functionalities did not affect the porous morphology, which was further observed from the SEM and

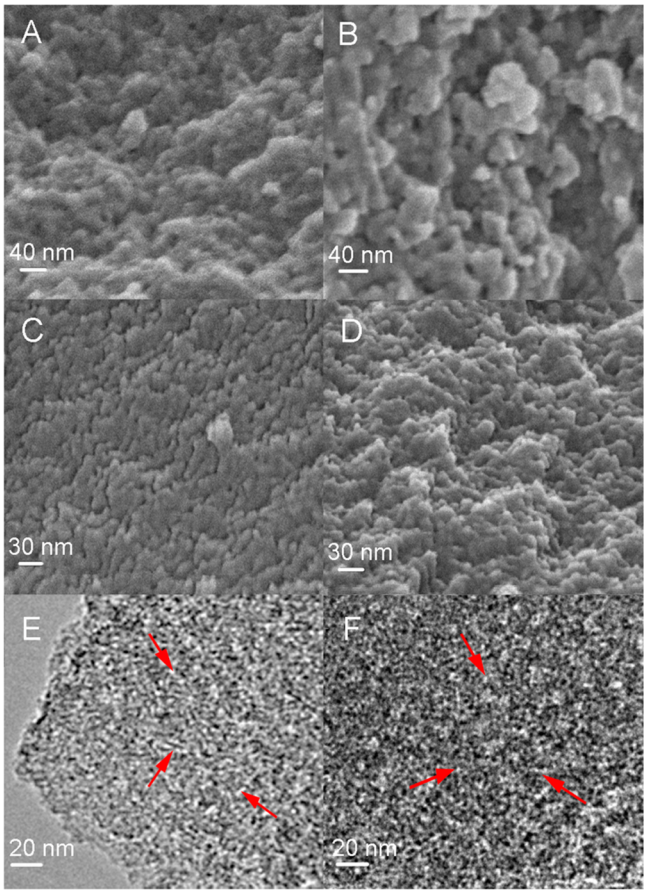

Figure 1. Scanning electron microscopy (SEM) images of (A) MOG, (B) PPy@MOG, (C) MOG-C, and (D) N@MOG-C. Also shown are transmission electron microscopy (TEM) images of (E) MOG-C and (F) N@MOG-C.

TEM images of MOG-C (see Figures 1C and 1E) and N@MOG-C (Figures 1D and 1F). In addition, the N@MOG-C kept the high degree of porosity of N@MOG (Figures 1B, 1D, and 1F), which suggested that the porous structure was sustained during the pyrolysis process. The TEM images exhibited that the porous carbon matrix consisted of interconnected nanoparticles, which were arrowed in Figures 1E and 1F, which indicated that the resulting N@MOG-C possessed a large specific surface area and high surface reaction activity.

The doping of nitrogen in carbon material was confirmed by XPS spectra. As shown in Figure 2A, only N@MOG-C showed the N 1s peak (curve b), suggesting the successful nitrogen doping in N@MOG-C. The high-resolution scan showed a broad peak of N 1s, indicated the presence of two forms of nitrogen of pyrrolic N at 400.5 eV (pink) and pyridinic N at 399.5 eV (green) (Figure 2A, inset).

The gel matrix structure of PPy@MOG was observed by powder X-ray diffraction (Figure 2B, curve b), which exhibited well-recognized diffraction patterns with the reflection peaks similar to those of MOF structure MIL-100 (Al) (curve a),[35] implying that the as-synthesized PPy@MOG retained the crystalline and ordered porous structure of MOF. The high diffraction intensity of PPy@MOG should be attributed to its large grains observed in Figure 1B. In addition, considering the inherent correlation between MOF and MOG with comparable bonding connectivity but different structural regularity, broad

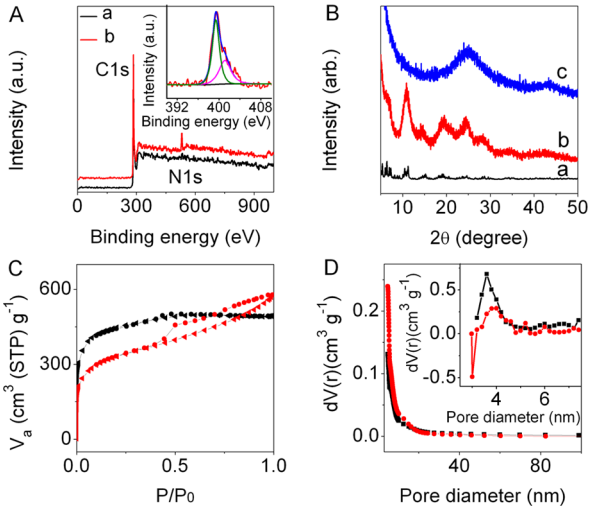

Figure 2. (A) XPS spectra of (a) MOG-C and (b) N@MOG-C. Inset in panel A shows high-resolution XPS analyses of N 1s in N@MOG-C (red), pyrrolic N (pink), pyridinic N (green), and fitted curve (blue). (B) XRD patterns of (a) MIL-100 (Al), (b) PPy@MOG, and (c) N@MOG-C. (C) N_2 adsorption (●)/desorption (◀) isotherms of MOG-C (red) and N@MOG-C (black). (D) Pore size distribution of MOG-C (red) and N@MOG-C (black). Inset in panel D shows an enlarged view of the pore size distribution.

peaks could be observed on the diffraction curve of PPy@MOG.[34] XRD experiment was further performed to check the composition of N@MOG-C (curve c), which showed two broad signals at ~24° and ~44°. These signals corresponded to the (002) and (100) planes of turbostratic carbon, indicating that the obtained N@MOG-C possessed an amorphous structure. Moreover, no alumina peak was observed, suggesting the alumina was totally removed by the HF treatment.

Nitrogen adsorption−desorption isotherms of the porous carbon materials are shown in Figure 2C. Compared with MOG-C (data indicated in red), N@MOG-C (data indicated in black) exhibited a smaller mesoporous hysteresis loop with adsorption and desorption branches at high relative pressures, indicating that N@MOG-C possessed less mesopores than MOG-C. The surface area of N@MOG-C determined by Brunauer−Emmett−Teller (BET) testing was 1542.6 $m^2\ g^{-1}$, which was 1.3 times higher than that of MOG-C. In addition, the pore size distribution of N@MOG-C was in a mesoporous range (Figure 2D), which ranged from 3.5 nm to 30 nm, indicating that the mesopores were formed as the interspaces among the packed particles in N@MOG-C. Therefore, the N@MOG-C possessed high BET surface area and appropriate pore diameter and could be a promising electrode modification material.

Electrochemical Characterization of N@MOG-C Modified Electrode. The electrochemical features of the N@MOG-C-modified electrode were examined in 5 mM $Fe(CN)_6^{3-/4-}$ containing 0.1 M KCl. As shown in Figure 3A, a pair of quasi-reversible redox peaks of $Fe(CN)_6^{3-/4-}$ with a peak separation (ΔE_p) of 181 mV were obtained at a bare GCE (curve a). When the electrode was coated with IL (curve b), the peak currents increased and the ΔE_p reduced to 123 mV, which suggested that the positively charged IL with good conductivity was favorable for the approach of $Fe(CN)_6^{3-/4-}$. Compared with the cyclic voltammogram of IL/GCE, a significant enhancement of the peak currents was observed at IL-N@

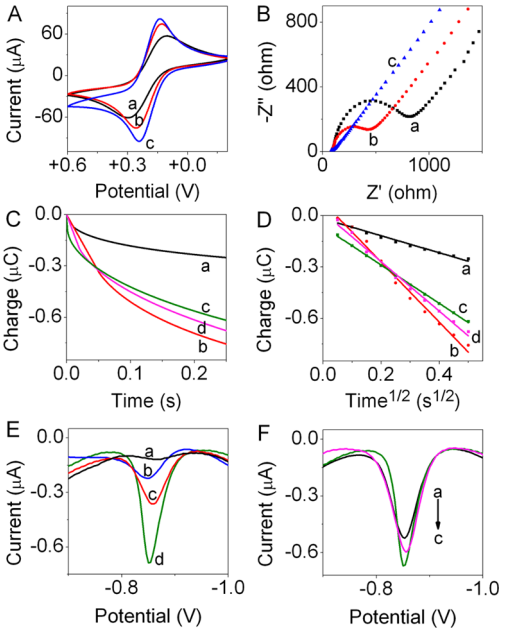

Figure 3. (A) Cyclic voltammograms and (B) EIS spectra of (a) bare GCE, (b) IL-modified GCE, and (c) IL-N@MOG-C-modified GCE in the solution containing 5 mM $Fe(CN)_6^{3-/4-}$ and 0.1 M KCl. Plots of (C) $Q-t$ and (D) $Q-t^{1/2}$ curves of GCE (curve a) and modified GCEs (IL-N@MOG-C (curve b), IL-TEPA@RGO (curve c), and IL-MWCNTs (curve d)) in 0.1 mM $K_3[Fe(CN)_6]$ containing 0.1 M KCl. (E) Square-wave anodic stripping voltammetry (SWASV) analyses of (a) bare GCE (b), IL-modified GCE, (c) IL-MOG-C-modifed GCE, and (d) IL-N@MOG-C modified GCE in 0.1 M acetate buffer (pH 5.0) containing 0.1 μM Cd(II). (F) SWASVs of modified GCE ((a) IL-TEPA@RGO, (b) IL-MWCNTs, and (c) IL-N@MOG-C) in 0.1 M acetate buffer (pH 5.0) containing 0.1 μM Cd(II).

MOG-C/GCE (curve c), indicating that N@MOG-C could accelerate the electron transfer.

EIS measurements were performed to examine the electron-transfer resistance (R_{et}) of the N@MOG-C-modified electrode (Figure 3B). In a typical EIS, the diameter of semicircle equals to R_{et}, which reflects the electron transfer kinetics of the redox probe at the electrode surface. The IL/GCE showed a much smaller R_{et} (curve b) than bare GCE (curve a), which implied that IL was an excellent electric conducting material to accelerate the electron transfer. After the IL-N@MOG-C was modified on the GCE, a significant decrease in R_{et} was observed (curve c in Figure 3B; also see Figure S2 in the Supporting Information). This result could be attributed to the excellent conductivity of N@MOG-C. The active electrode area of IL-N@MOG-C/GCE could be measured with chronocoulometry (Figure 3C), using 0.1 mM $K_3[Fe(CN)_6]$, whose diffusion coefficient (D) is 7.6×10^{-6} cm^2 s^{-1},[36] based on eq 1:[37]

$$Q(t) = \frac{2nFAcD^{1/2}t^{1/2}}{\pi^{1/2}} + Q_{dl} + Q_{ads} \quad (1)$$

where n is the electron transfer number; A is the effective surface area of the working electrode; c is the concentration of substrate; D is the diffusion coefficient; Q_{dl} is the double layer charge, which could be eliminated by background subtraction; and Q_{ads} is the Faradaic charge consumed by adsorbed species. Other symbols have their usual meaning. The plots of Q vs $t^{1/2}$ are shown in Figure 3D. The effective area of IL-N@MOG-C/GCE was calculated to be 0.0586 cm^2, which was much higher than 0.03734 cm^2 of IL-TEPA@RGO/GCE, 0.04815 cm^2 of IL-MWCNTs/GCE, and 0.0166 cm^2 of bare GCE. Such a high effective area of IL-N@MOG-C/GCE was favorable for the design of a highly sensitive sensing platform for heavy metal ions. This advantage could be demonstrated from the square-wave anodic stripping voltammetry (SWASV) responses of 0.1 μM Cd(II) at different electrodes. The stripping peak current of IL-N@MOG-C/GCE was obviously larger than those of bare GCE, IL/GCE, and IL-MOG-C/GCE (Figure 3E). In addition, compared with the IL-TEPA@RGO/GCE (curve a) and IL-MWCNTs/GCE (curve b), the IL-N@MOG-C-modified GCE (curve c) presented a higher and sharper peak current (Figure 3F). The result could be attributed to the better absorbability and conductivity of N@MOG-C than commercial RGO and MWCNTs toward the target heavy-metal ion, indicating that the developed N-doped porous carbon could be a promising electrode material for the detection of metal ions.

Optimization of Detection Conditions. In order to get the maximum sensitivity for trace heavy-metal detection with the IL-N@MOG-C-modified GCE, the preparation of the modified electrode and the detection conditions (such as the amount of N@MOG-C, solution pH, deposition potential, and time) were optimized. With the increasing amount of N@MOG-C in 50 μL of IL, the SWASV response of 0.1 μM Cd(II) at the obtained modified electrode increased and reached the maximum value at 1.0 mg of N@MOG-C (Figure 4A).

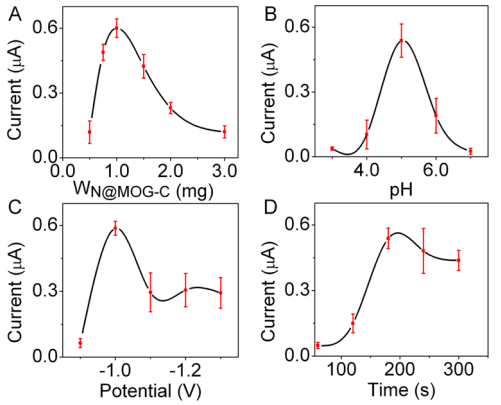

Figure 4. Influence of (A) mass effect of N@MOG-C, (B) pH value, (C) deposition potential and (D) deposition time on SWASV responses of IL-N@MOG-C modified GCE in acetate buffer (pH 5.0) containing 0.1 μM Cd(II). Results were expressed as the average of three independent experiments. Error bars represent standard deviations (SD, σ).

However, the further increase of the mass resulted in a decrease of the SWASV peak current due to the lower ratio of IL, which resulted in a loss of film stability and the decrease of electrical connectivity of the modification film. Therefore, 1.0 mg of N@MOG-C in 50 μL of IL was chosen for electrode modification.

The effect of pH on the voltammetric response was examined from pH 3.0 to pH 7.0 (Figure 4B), which showed the maximum response at pH 5.0. Thus, pH 5.0 was selected as the optimal pH for stripping voltammetric measurements. When the deposition potential shifted from −0.9 V to −1.3 V, the stripping peak current for Cd(II) increased and reached a maximum at −1.0 V (Figure 4C). The response decrease at deposition potentials more negative than −1.0 V was due to the competitive generation of H_2. Thus, −1.0 V was chosen as the

optimal deposition potential, at which the response reached the saturated value at a deposition time of 180 s (Figure 4D).

Analytical Performance. The IL-N@MOG-C modified electrode was used to determine Cd(II) with SWASV. The stripping peak current of Cd(II) increased proportionally with the increasing concentration of Cd(II) (Figure 5A). The plot of peak current versus concentration exhibited good linearity in the range of 0.025−5 μM, with a correlation coefficient of 0.9905 (see Figure 5B). The detection limit at 3σ was calculated to be 2.2 nM, which was much lower than the limited value of 3.0 μg L^{-1} in drinking water permitted by the World Health Organisation (WHO).[38] The analytical performance was also compared with other modified electrodes reported previously, which were summarized in Table 1. The detection limit of the proposed method was comparable to other electrochemical Cd(II) detection methods.

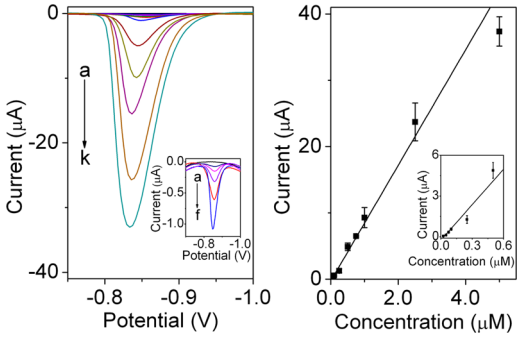

Figure 5. (A) SWASV responses of the IL-N@MOG-C modified GCE to Cd(II) at concentrations of 0 (a), 0.025 (b), 0.05 (c), 0.075 (d), 0.1 (e), 0.25 (f), 0.5 (g), 0.75 (h), 1.0 (i), 2.5 (g), and 5.0 μM (k). (B) The corresponding calibration curve. Inset: 0.025−0.5 μM Cd(II). Results were expressed as the average of three independent experiments. Error bars represent standard deviations (SD, σ).

Determination of Cd(II) in Real Samples. The feasibility of the proposed method was investigated by detecting Cd(II) in natural water samples, including tap water and lake water (from Qinhuai River in Nanjing, China). All the samples were filtered through a 0.2 μm membrane prior to detection. These water samples did not showed any response of Cd(II), indicating that the concentration of Cd(II) was extremely low. Thus, different concentrations of Cd(II) were spiked into these samples for recovery evaluation. The SWASV responses and detection results are shown in Figure S3 and Table S1 in the Supporting Information), respectively. The average recoveries ranged from 102.9% to 95.0% for three determinations, addressing the good accuracy of the proposed method for Cd(II) detection in real samples.

The repeatability of the electrode was investigated by repetitively determining 0.1 μM Cd(II). The relative standard deviation (RSD) of peak currents was 5.3% (n = 15). The response sensitivity retained a value of more than 95% over 6 weeks. The reproducibility of the electrode preparation was also studied. Six electrodes were prepared from the same batch and evaluated by performing determination of the Cd(II). Here, the RSD value was 4.1%. The high stability and reproducibility indicated that the modified electrode was suitable for the analysis of real samples.

In respect of selectivity, the effect of various metal ions including Mg^{2+}, Fe^{3+}, Co^{2+}, Ni^{2+}, Zn^{2+}, Hg^{2+}, Pb^{2+}, Mn^{2+}, Cu^{2+}, and Al^{3+} at 10 μM on the determination of 0.1 μM Cd(II) was studied. Only high concentrations of Cu^{2+} and Hg^{2+} (>10 μM) were found to interfere heavily with the determination of Cd(II); the other metal ions had no influence, with deviations of <6%. Mercury ions could be reduced and form a film on the surface of electrode, which caused Cd(II) to be reduced more easily by forming an amalgam.[51] Consequently, the anodic stripping peak currents increased in the presence of Hg^{2+}. However, the SWASV signal for Cd(II) was significantly diminished in the presence of Cu^{2+}, likely because of the formation of a Cd−Cu intermetallic compound.[52] Therefore, ferricyanide was selected to exclude the interference of Cu^{2+}.

CONCLUSION

A nitrogen-doped porous carbon material, N@MOG-C, with a uniform interconnected structure, was synthesized with a metal−organic gel (MOG) template and applied as the electrode material for the sensitive detection of heavy-metal ions. The porous structure of N@MOG-C produced a highly effective area of the modified electrode, resulting in faster electron transfer kinetics than MOG-C and other commercial carbon materials. The N@MOG-C-modified electrode could detect the Cd ion with high sensitivity and good accuracy and selectivity. Benefiting from its porous structure and fast electron

Table 1. Comparison of the Electrodes Modified with N@MOG-C and Other Materials for the Detection of Cd(II)

electrode	modifier	detection range (μM)	limit of detection, LOD[a] (μM)	ref
CPE[b]	N-BDMP[c]	0.089−17.8	0.059	39
CPE	diacetyldioxime	0.25−25	0.04	40
CPE	antimony film	0.045−0.45	0.071	41
CPE	mesoporous silica SBA-15	0.6−30	0.08	42
SPCE[d]	bismuth film	0−0.62	0.00614	43
microelectrode	antimony film	0.18−0.89	0.0169	44
GCDE[e]	bismuth film	0.089−0.89	0.01245	45
GCE	Nafion-Bi film	0.018−0.53	0.00178	46
GCE	Nafion/SWNTs[f]	0.04−0.4	0.004	47
GCE	MWNTs	0.025−10	0.006	48
GCE	nano-SWy-2-AQ[g]	0.008−1	0.003	49
GCE	TCA[h]	0.2−50	0.02	50
GCE	N@MOG-C	0.025−5	0.0022	this work

[a]Limit of detection. [b]Carbon paste electrode. [c]Nitro benzoyl diphenylmethylenphosphorane. [d]Screen-printed carbon electrode. [e]Glassy carbon disc working electrode. [f]Single-walled carbon nanotubes. [g]Improved Na-montmorillonite nanoparticles and anthraquinone. [h]*p-tert*-butylthiacalix[4]arene.

transfer ability, N@MOG-C could be a promising electrode material for sensing other heavy-metal ions and molecules.

■ ASSOCIATED CONTENT

Supporting Information

Additional information as noted in text. This material is available free of charge via the Internet at http://pubs.acs.org.

■ AUTHOR INFORMATION

Corresponding Author

*Tel./Fax: +86-25-83593593. E-mail: hxju@nju.edu.cn.

Notes

The authors declare no competing financial interest.

■ ACKNOWLEDGMENTS

We gratefully acknowledge the National Special Project for Key Scientific Apparatus Development (No. 2012YQ170000302), National Basic Research Program (No. 2010CB732400), and National Natural Science Foundation of China (Nos. 21135002 and 21121091).

■ REFERENCES

(1) Kašuba, V.; Rozgaj, R.; Sarić, M. M.; Blanuša, M. Evaluation of Genotoxic Damage of Cadmium Chloride in Peripheral Blood of Suckling Wistar Rats. *J. Appl. Toxicol.* **2002**, *22*, 271−277.

(2) Abbaspour, A.; Mirahmadi, E.; Khalafi-Nejad, A.; Babamohammadi, S. A Highly Selective and Sensitive Disposable Carbon Composite PVC-Based Membrane for Determination of Lead Ion in Environmental Samples. *J. Hazard. Mater.* **2010**, *174*, 656−661.

(3) Huang, K. W.; Yu, C. J.; Tseng, W. L. Sensitivity Enhancement in the Colorimetric Detection of Lead (II) Ion Using Gallic Acid-Capped Gold Nanoparticles: Improving Size Distribution and Minimizing Interparticle Repulsion. *Biosens. Bioelectron.* **2010**, *25*, 984−989.

(4) McGaw, E. A.; Swain, G. M. A Comparison of Boron-Doped Diamond Thin-Film and Hg-Coated Glassy Carbon Electrodes for Anodic Stripping Voltammetric Determination of Heavy Metal Ions in Aqueous Media. *Anal. Chim. Acta* **2006**, *575*, 180−189.

(5) Aragay, G.; Merkoçi, A. Nanomaterials Application in Electrochemical Detection of Heavy Metals. *Electrochim. Acta* **2012**, *84*, 49−61.

(6) Wang, J. Stripping Analysis at Bismuth Electrodes: A Review. *Electroanalysis* **2005**, *17*, 1341−1346.

(7) Aragay, G.; Pons, J.; Merkoçi, A. Enhanced Electrochemical Detection of Heavy Metals at Heated Graphite Nanoparticle-Based Screen-Printed Electrodes. *J. Mater. Chem.* **2011**, *21*, 4326−4331.

(8) Li, S. L.; Xu, Q. Metal-Organic Frameworks as Platforms for Clean Energy. *Energy Environ. Sci.* **2013**, *6*, 1656−1683.

(9) Liu, H.; Liu, Y.; Li, Y.; Tang, Z.; Jiang, H. Metal-Organic Framework Supported Gold Nanoparticles as a Highly Active Heterogeneous Catalyst for Aerobic Oxidation of Alcohols. *J. Phys. Chem. C* **2010**, *114*, 13362−13369.

(10) Furukawa, H.; Gándara, F.; Zhang, Y. B.; Jiang, J.; Queen, W. L.; Hudson, M. R.; Yaghi, O. M. Water Adsorption in Porous Metal-Organic Frameworks and Related Materials. *J. Am. Chem. Soc.* **2014**, *136*, 4369−4381.

(11) Furukawa, H.; Cordova, K. E.; O'Keeffe, M.; Yaghi, O. M. The Chemistry and Applications of Metal-Organic Frameworks. *Science* **2013**, *341*, 1230444-1−1230444-12.

(12) Wang, C.; Liu, D.; Lin, W. Metal-Organic Frameworks as A Tunable Platform for Designing Functional Molecular Materials. *J. Am. Chem. Soc.* **2013**, *135*, 13222−13234.

(13) Talin, A. A.; Centrone, A.; Ford, A. C.; Foster, M. E.; Stavila, V.; Haney, P.; Kinney, R. A.; Szalai, V.; El Gabaly, F.; Yoon, H. P. Tunable Electrical Conductivity in Metal-Organic Framework Thin-Film Devices. *Science* **2014**, *343*, 66−69.

(14) Lee, H. J.; Choi, S.; Oh, M. Well-Dispersed Hollow Porous Carbon Spheres Synthesized by Direct Pyrolysis of Core-Shell Type Metal-Organic Frameworks and Their Sorption Properties. *Chem. Commun.* **2014**, *50*, 4492−4495.

(15) Li, J.; Chen, Y.; Tang, Y.; Li, S.; Dong, H.; Li, K.; Han, M.; Lan, Y. Q.; Bao, J.; Dai, Z. Metal-Organic Framework Templated Nitrogen and Sulfur Co-Doped Porous Carbons as Highly Efficient Metal-Free Electrocatalysts for Oxygen Reduction Reactions. *J. Mater. Chem. A* **2014**, *2*, 6316−6319.

(16) Hu, M.; Reboul, J.; Furukawa, S.; Torad, N. L.; Ji, Q.; Srinivasu, P.; Ariga, K.; Kitagawa, S.; Yamauchi, Y. Direct Carbonization of Al-Based Porous Coordination Polymer for Synthesis of Nanoporous Carbon. *J. Am. Chem. Soc.* **2012**, *134*, 2864−2867.

(17) Chaikittisilp, W.; Hu, M.; Wang, H.; Huang, H. S.; Fujita, T.; Wu, K. C. W.; Chen, L. C.; Yamauchi, Y.; Ariga, K. Nanoporous Carbons through Direct Carbonization of a Zeolitic Imidazolate Framework for Supercapacitor Electrodes. *Chem. Commun.* **2012**, *48*, 7259−7261.

(18) Xu, G.; Ding, B.; Shen, L.; Nie, P.; Han, J.; Zhang, X. Sulfur Embedded in Metal Organic Framework-Derived Hierarchically Porous Carbon Nanoplates for High Performance Lithium−Sulfur Battery. *J. Mater. Chem. A* **2013**, *1*, 4490−4496.

(19) Qiu, B.; Pan, C.; Qian, W.; Peng, Y.; Qiu, L.; Yan, F. Nitrogen-Doped Mesoporous Carbons Originated From Ionic Liquids as Electrode Materials for Supercapacitors. *J. Mater. Chem. A* **2013**, *1*, 6373−6378.

(20) Liu, B.; Shioyama, H.; Jiang, H.; Zhang, X.; Xu, Q. Metal-Organic framework (MOF) as a Template for Syntheses of Nanoporous Carbons as Electrode Materials for Supercapacitor. *Carbon* **2010**, *48*, 456−463.

(21) Jiang, H. L.; Liu, B.; Lan, Y. Q.; Kuratani, K.; Akita, T.; Shioyama, H.; Zong, F.; Xu, Q. From Metal-Organic Framework to Nanoporous Carbon: Toward a Very High Surface Area and Hydrogen Uptake. *J. Am. Chem. Soc.* **2011**, *133*, 11854−11857.

(22) Xia, W.; Zhang, X.; Xu, L.; Wang, Y.; Lin, J.; Zou, R. Facile and Economical Synthesis of Metal-Organic Framework MIL-100 (Al) Gels for High Efficiency Removal of Microcystin-LR. *RSC Adv.* **2013**, *3*, 11007−11013.

(23) Xiang, S.; Li, L.; Zhang, J.; Tan, X.; Cui, H.; Shi, J.; Hu, Y.; Chen, L.; Su, C. Y.; James, S. L. Porous Organic-Inorganic Hybrid Aerogels Based on Cr^{3+}/Fe^{3+} and Rigid Bridging Carboxylates. *J. Mater. Chem.* **2012**, *22*, 1862−1867.

(24) Lohe, M. R.; Rose, M.; Kaskel, S. Metal-Organic Framework (MOF) Aerogels with High Micro- and Macroporosity. *Chem. Commun.* **2009**, 6056−6058.

(25) Fages, F. Metal Coordination to Assist Molecular Gelation. *Angew. Chem., Int. Ed.* **2006**, 1680−1682.

(26) Leong, W. L.; Tam, A. Y. Y.; Batabyal, S. K.; Koh, L. W.; Kasapis, S.; Yam, V. W. W.; Vittal, J. J. Fluorescence Enhancement of Coordination Polymeric Gel. *Chem. Commun.* **2008**, 3628−3630.

(27) De Paoli, G.; Džolic, Z.; Rizzo, F.; De Cola, L.; Voegtle, F.; Mueller, W. M.; Richardt, G.; Žinic, M. Reversible Luminescent Gels Containing Metal Complexes. *Adv. Funct. Mater.* **2007**, *17*, 821−828.

(28) Zhang, J.; Su, C. Y. Metal-Organic Gels: From Discrete Metallogelators to Coordination Polymers. *Coord. Chem. Rev.* **2013**, *257*, 1373−1408.

(29) Mallick, A.; Schön, E. M.; Panda, T.; Sreenivas, K.; Díaz, D. D.; Banerjee, R. Fine-Tuning the Balance between Crystallization and Gelation and Enhancement of CO_2 Uptake on Functionalized Calcium Based MOFs and Metallogels. *J. Mater. Chem.* **2012**, *22*, 14951−14963.

(30) Piepenbrock, M. O. M.; Lloyd, G. O.; Clarke, N.; Steed, J. W. Metal-and Anion-Binding Supramolecular Gels. *Chem. Rev.* **2009**, *110*, 1960−2004.

(31) Liu, Y. R.; He, L.; Zhang, J.; Wang, X.; Su, C. Y. Evolution of Spherical Assemblies to Fibrous Networked Pd (II) Metallogels from a Pyridine-Based Tripodal Ligand and Their Catalytic Property. *Chem. Mater.* **2009**, *21*, 557−563.

(32) Nune, S. K.; Thallapally, P. K.; McGrail, B. P. Metal Organic Gels (MOGs): A New Class of Sorbents for CO_2 Separation Applications. *J. Mater. Chem.* **2010**, *20*, 7623−7625.
(33) Li, L.; Xiang, S.; Cao, S.; Zhang, J.; Ouyang, G.; Chen, L.; Su, C. Y. A Synthetic Route to Ultralight Hierarchically Micro/Mesoporous Al(III)-Carboxylate Metal-Organic Aerogels. *Nat. Commun.* **2013**, *4*, 1774−1782.
(34) Xia, W.; Qiu, B.; Xia, D.; Zou, R. Facile Preparation of Hierarchically Porous Carbons from Metal-Organic Gels and Their Application in Energy Storage. *Sci. Rep.* **2013**, *3*, 1935−1941.
(35) Volkringer, C.; Popov, D.; Loiseau, T.; Férey, G.; Burghammer, M.; Riekel, C.; Haouas, M.; Taulelle, F. Synthesis, Single-Crystal X-ray Microdiffraction, and NMR Characterizations of the Giant Pore Metal-Organic Framework Aluminum Trimesate MIL-100. *Chem. Mater.* **2009**, *21*, 5695−5697.
(36) Adams, R. N. *Electrochemistry at Solid Electrodes*; Marcel Dekker: New York, 1969.
(37) Anson, F. Application of Potentiostatic Current Integration to the Study of the Adsorption of Cobalt(III)-(Ethylenedinitrilo (tetraacetate) on Mercury Electrodes. *Anal. Chem.* **1964**, *36*, 932−934.
(38) Cerutti, S.; Silva, M. F.; Gásquez, J. A.; Olsina, R. A.; Martinez, L. D. On-line Preconcentration/Determination of Cadmium in Drinking Water on Activated Carbon Using 8-Hydroxyquinoline in a Flow Injection System Coupled to an Inductively Coupled Plasma Optical Emission Spectrometer. *Spectrochim. Acta, Part B* **2003**, *58*, 43−50.
(39) Afkhami, A.; Madrakian, T.; Sabounchei, S. J.; Rezaei, M.; Samiee, S.; Pourshahbaz, M. Construction of a Modified Carbon Paste Electrode for the Highly Selective Simultaneous Electrochemical Determination of Trace Amounts of Mercury (II) and Cadmium (II). *Sens. Actuators B* **2012**, *161*, 542−548.
(40) Hu, C.; Wu, K.; Dai, X.; Hu, S. Simultaneous Determination of Lead(II) and Cadmium(II) at a Diacetyldioxime Modified Carbon Paste Electrode by Differential Pulse Stripping Voltammetry. *Talanta* **2003**, *60*, 17−24.
(41) Tesarova, E.; Baldrianova, L.; Hocevar, S. B.; Svancara, I.; Vytras, K.; Ogorevc, B. Anodic Stripping Voltammetric Measurement of Trace Heavy Metals at Antimony Film Carbon Paste Electrode. *Electrochim. Acta* **2009**, *54*, 1506−1510.
(42) Zhang, P.; Dong, S.; Gu, G.; Huang, T. Simultaneous Determination of Cd^{2+}, Pb^{2+}, Cu^{2+} and Hg^{2+} at a Carbon Paste Electrode Modified with Ionic Liquid-Functionalized Ordered Mesoporous Silica. *Bull. Korean Chem. Soc.* **2010**, *31*, 2949−2954.
(43) MotoMIzu, S.; Dungchai, W.; Chailapakul, O.; Motomizu, S. Determination of Trace Heavy Metals by Sequential Injection-Anodic Stripping Voltammetry Using Bismuth Film Screen-Printed Carbon Electrode. *Anal. Sci.* **2008**, *24*, 589−594.
(44) Slavec, M.; Hocevar, S. B.; Baldrianova, L.; Tesarova, E.; Svancara, I.; Ogorevc, B.; Vytras, K. Antimony Film Microelectrode for Anodic Stripping Measurement of Cadmium(II), Lead(II) and Copper(II). *Electroanalysis* **2010**, *22*, 1617−1622.
(45) Siriangkhawut, W.; Pencharee, S.; Grudpan, K.; Jakmunee, J. Sequential Injection Monosegmented Flow Voltammetric Determination of Cadmium and Lead Using a Bismuth Film Working Electrode. *Talanta* **2009**, *79*, 1118−1124.
(46) Kefala, G.; Economou, A. Polymer-Coated Bismuth Film Electrodes for the Determination of Trace Metals by Sequential-Injection Analysis/Anodic Stripping Voltammetry. *Anal. Chim. Acta* **2006**, *576*, 283−289.
(47) Sun, D.; Xie, X.; Cai, Y.; Zhang, H.; Wu, K. Voltammetric Determination of Cd^{2+} Based on the Bifunctionality of Single-Walled Carbon Nanotubes−Nafion Film. *Anal. Chim. Acta* **2007**, *581*, 27−31.
(48) Wu, K.; Hu, S.; Fei, J.; Bai, W. Mercury-Free Simultaneous Determination of Cadmium and Lead at a Glassy Carbon Electrode Modified with Multi-Wall Carbon Nanotubes. *Anal. Chim. Acta* **2003**, *489*, 215−221.
(49) Yuan, S.; Chen, W.; Hu, S. Simultaneous Determination of Cadmium(II) and Lead(II) with Clay Nanoparticles and Anthraquinone Complexly Modified Glassy Carbon Electrode. *Talanta* **2004**, *64*, 922−928.
(50) Zheng, H.; Yan, Z.; Dong, H.; Ye, B. Simultaneous Determination of Lead and Cadmium at a Glassy Carbon Electrode Modified with Langmuir-Blodgett Film of *p-tert*-butylthiacalix[4]arene. *Sens. Actuators B* **2007**, *120*, 603−609.
(51) Schiewe, J.; Oldham, K. B.; Myland, J. C.; Bond, A. M.; Vicente-Beckett, V. A.; Fletcher, S. Linear-Scan Anodic Stripping Voltammetry with Thin-Film Electrodes: Theory of the Stripping Stage and Experimental Tests. *Anal. Chem.* **1997**, *69*, 2673−2681.
(52) Grim, R. J. Catalytic Activity of an Intermetallic Compound of Cadmium and Copper in the Vapor-Phase Reduction of Nitrobenzene. *J. Phys. Chem.* **1942**, *46*, 464−469.